Environmental Technology & Innovation 40 (2025) 104583

Contents lists available at ScienceDirect

Environmental Technology & Innovation

journal homepage: www.elsevier.com/locate/eti

Single particle identification and automated classification of small (<10μm) microplastics using cathodoluminescence

Elena M. Höppener [a,*], Laurine E.A. Yoe [a], Luke A. Parker [a], Edward van Amelrooij [b], Sieger Henke [a], Alexandra H. Leighton [a]

[a] TNO Environmental Modelling, Sensing, and Analysis, Princetonlaan 6-8, Utrecht 3584 CB, the Netherlands
[b] KNMI, the Netherlands

ARTICLE INFO

Keywords:
microplastics
cathodoluminescence
single-particle detection
random forest classifier

ABSTRACT

Despite growing awareness of the negative impacts of plastic pollution, its production and resulting waste continue to increase. Once in the environment, plastic waste breaks down into microplastic (MP) particles, which have been detected in various environmental and biological matrices, including air, water, sediment, blood, and brain tissue. However, the full extent of the problem remains unclear due to limitations in current detection techniques. This paper builds on our previous work with Scanning Electron Microscopy coupled with Cathodoluminescence (SEM-CL) and demonstrated that small particles of commonly used plastics exhibit unique CL spectra. After optimizing signal parameters, we successfully collected over 200 CL spectra of test materials (1–10 μm) of polyethylene (PE), polypropylene (PP), polyamide (PA), polystyrene (PS), and polyethylene terephthalate (PET). Principal component analysis (PCA) confirmed the uniqueness of CL spectra for differentiating plastic types. A random forest classifier (RFC) was trained on the first 10 principal components (PCs) and achieved 94 % accuracy. To minimize pre-processing, a second RFC was trained on normalised CL spectra, also achieving 94 % accuracy. By applying a certainty threshold, untrained contaminants such as kaolin, talc, and titanium dioxide were separated from the plastics. This work laid the foundation for a robust detection tool for single particle identification and automated classification of microplastics smaller than 10 μm using SEM-CL.

1. Introduction

Despite increased awareness of the negative impacts of plastic pollution, the amount of plastic waste in our environment continues

Abbreviations: ANN, Artificial neural network; BI, Beam intensity; BSE, Backscattered electron; CARS, Coherent anti-Stokes Raman scattering; CL, Cathodoluminescence; Da, Average particle diameter; EDX, Energy-dispersive X-ray spectroscopy; FTIR, Fourier-transform infrared spectroscopy; HDPE, High-density polyethylene; KeV, Kiloelectronvolt; LDPE, Low-density polyethylene; MPs, Microplastics; Mt, Million tonnes; Nm, Nanometer; PA, Polyamide; PCA, Principal component analysis; PCs, Principal components; PE, Polyethylene; PET, Polyethylene terephthalate; PP, Polypropylene; PS, Polystyrene; Pyr-GCMS, Pyrolysis gas chromatography mass spectrometry; RFC, Random forest classifier; SEM, Scanning electron microscopy; SEM-CL, Scanning electron microscopy coupled with cathodoluminescence; SE, Secondary electron; SI, Supplementary Information; SLS, Static light scattering; SRS, Stimulated Raman scattering; TiO2, Titanium dioxide; XRF, X-ray fluorescence; μm, Micrometer micron.

* Corresponding author.
E-mail address: elena.hoppener@tno.nl (E.M. Höppener).

https://doi.org/10.1016/j.eti.2025.104583
Received 6 August 2025; Received in revised form 20 October 2025; Accepted 21 October 2025
Available online 25 October 2025

to increase (OECD, 2022). Plastic production has doubled over the past decades, from 200 million tonnes (Mt) in 2000–413 Mt in 2023 (Plastic Europe, 2024). Current waste management and plastic recycling activities still fall far short of the circular ideal, as only 9 % of plastic is successfully recycled worldwide (OECD, 2022). Once in the environment, plastic waste can fragment into smaller pieces through various processes, generating microplastics (MPs) as a result (Geyer et al., 2017; ISO/TR 21960:2020en, 2022). The presence of MPs provides serious grounds for concern, both through direct mechanical and chemical dangers to human health as well as via adverse effects on ecosystems threatening food security (Leslie and Depledge, 2020; Vethaak and Legler, 2021; Nair and Perumal, 2022). Microplastics have been shown to affect survival and reproduction in various organisms (Zimmermann et al., 2020; Wei et al., 2022). Adhering to the precautionary principle requires that we minimise their release, (Rathenau, 2020) and the EU Zero Pollution Action Plan has set a 30 % reduction target of microplastic release by 2030 (European Commission, 2021, 2021).

The presence of this environmental pollutant has been widely investigated, with MPs being detected in air (Gasperi et al., 2018; Wright et al., 2021), water (Koelmans et al., 2019; Schymanski et al., 2021), sediment (Phuong et al., 2021; Uddin et al., 2021), aquatic organisms (Sunny et al., 2025), human blood (Leslie et al., 2022) and brain tissue (Campen et al., 2024). Detailed characterisation of these particles is crucial, as the harm caused by MPs is determined by their constituent polymer, their size (Thornton Hampton et al., 2022), and any additives or surfactants that may leach from the particle. As smaller particles are more likely to be ingested and to subsequently translocate within an organism (Thornton Hampton et al., 2022), they are particularly important to identify (Thornton Hampton et al., 2022). However, characterisation is particularly challenging for smaller MPs of under 10 μm. This is largely due to the additional level of difficulty in single particle detection, identification and quantification of smaller particles also comes with unique challenges, largely due to the (spatial) detection limits of common analytical methods (Mandemaker and Meirer, 2023).

The most predominantly used analytical techniques for MPs are Raman spectroscopy for single-particle detection and pyrolysis gas chromatography mass spectrometry (pyr-GCMS) for mass concentrations. Although pyr-GCMS based techniques are capable of quantifying the total mass of nanoplastics in various (environmental) matrices, the technique offers no insight into the number, size and shape of the particles, thus providing us with little information on the physicochemical properties of nanoplastics at particle level (Zhou et al., 2025). Although Raman spectroscopy techniques are capable of identifying the individual plastic particles, they remain unsuitable for the detection of nanoplastics due to poor sensitivity and spatial resolution (Pei et al., 2023). To a degree, these drawbacks can be overcome using enhanced techniques such as coherent anti-Stokes Raman scattering (CARS) and stimulated Raman scattering (SRS) resulting in, for example, a Raman enhancement factor maximised to 10^8 (Qian et al., 2023). Although these advances are promising, challenges remain due fluorescence interference and troubles measuring dark coloured materials using Raman. Furthermore, even the best optical microscopes are diffraction-limited due to the physics of light diffraction, restricting optical systems to lateral resolution limit of approximately ~200 nm (Nikon, 2025).

Scanning electron microscopy coupled with cathodoluminescence (SEM-CL) combines spectroscopic identification with the high spatial resolution of an electron microscope. Cathodoluminescence (CL) refers to the emission of photons resulting from the excitation of a material by electrons. To achieve optimal spatial resolution, CL signals are typically acquired within a scanning electron microscope (SEM). Not only can it be used to study the microstructures of various materials, including perovskites, (Li et al., 2025) ceramics, (Palamara et al., 2020) and non-metallic inclusions, (Jiang et al., 2024) it also has the potential to perform single particle detection of plastic particles in various matrices (Mandemaker and Meirer, 2023). Adding to that, since SEM-CL probes the electronic structure and microstructural features of materials—rather than elemental composition as in energy-dispersive X-ray spectroscopy (EDX), or molecular bonding as in FTIR and Raman—it provides a complementary insight for the identification and characterization of plastic materials. In theory, the limit of detection for this technique is constrained by the size of the electron beam, making it possible to probe structures ranging from tens of nanometers to several millimeters—covering both the nanoplastic (tens of nanometers to 1 μm) and microplastic (1 μm to 5 mm) size ranges. In our previous work we demonstrated that macro- and microplastics (diameters around 100 μm) of common polymer types such as HDPE, LDPE, PP, PA, PS and PET could be classified with high accuracy (>97 %) based on their CL spectra (Höppener et al., 2023). For these reasons we hypothesised that this powerful analytical technique could be applied to even smaller plastic particles, down to the nanoscale. Yet some challenges for the applicability of this technique remained unanswered such as the potential for beam-induced damage to the sample and the low sensitivity for smaller particles showing the need to further investigate the limitations and capabilities of this technique.

Here, we investigated the applicability of this novel technique for the detection of small microplastics (1–10 μm). To achieve this we extended the spectral database with CL spectra of reference particles with sizes between 1 – 10 μm of (HD/LD)PE, PP, PA, PS and PET, tuning the acquisition parameters for successful small microplastic spectral acquisition. We used this database to train and test a random forest classifier for MPs, improving upon our previous approach by using a method that requires less computational power and very little data preprocessing. With this work, we hope to address the challenges that are accompanied with analysing small MPs using SEM-CL and create a foundation for a robust tool for microplastics researchers to quickly identify particle size and polymer.

2. Materials and methods

2.1. Materials

The microplastic types studied in this work were polyethylene (PE), polyamide (PA), polyethylene terephthalate (PET), polystyrene (PS) and polypropylene (PP). The particles used in this work were produced as part of multiple projects where microplastics particles were produced; BRIGID, MOMENTUM and MOMENTUM2.0 projects. PE, PET, PS and PP microplastics were received as powders from Nanofract AG (Magdeburg, Germany) with a broad size distribution. PA, PET and PP were further processed into smaller particles by TNO using a production protocol described in Parker et al.(2023). Detailed characterisation (XRF, SLS, SEM) of the particles can be

accessed from Zenodo (Parker et al., 2024). For each plastic type at least 40 different particles were measured with SEM-CL. A summary of the measured particles along with the average particle diameter (Da) per plastic type is provided in Table 1. Kaolin and Nanotalc were purchased directly as powders at SIGMA ALDRICH. The titanium dioxide (TiO_2) studied in this work was NM-101 and obtained from JRC (Rasmussen et al., 2014).

2.2. Sample preparation

Samples for SEM analyses were prepared by bringing a small amount of the sample with particles in a 1:1 solution of MilliQ and ethanol. The suspensions were filtered under reduced pressure (200 mbar) over a 25 mm diameter gold coated polycarbonate filters with pore sizes of 0.8 μm or 0.4 μm (TJ Environmental). After filtration, the filter was transferred onto an aluminium SEM-stub covered with a double sided carbon coated tape (JEOL). The samples were coated with a thin conductive film of carbon using a carbon evaporator (Quorum Q150 T carbon evaporator) to make the samples electronically conductive.

2.3. SEM-CL set up and measurements

Cathodoluminescence (CL) measurements were conducted within a Tescan MAIA III GMH field emission scanning electron microscope (SEM). Spectral data were acquired using a Delmic SPARC-Spectral system, equipped with a high-resolution CCD camera (Andor Newton DU920P) mounted on a SPARC ATM spectrograph. Light emission was collected via an aluminium paraboloid mirror with an acceptance angle of 1.49π steradians. The spectrograph featured a motorized entrance slit and a turret housing two interchangeable diffraction gratings. The CL experiments were performed using the protocol described in Höppener et al.(2023). Here, the spectra were recorded using hyperspectral imaging mode with a VIS-NIR optical module optimized for the 400–1000 nm wavelength range, providing a spectral resolution of 0.83 nm/pixel. For the measurements regarding particles smaller than 10 μm, key parameters were optimized accordingly. A reduced beam energy of 5 kV (compared to 15 kV) and a beam intensity setting of three were applied to minimize beam-induced damage while ensuring sufficient excitation. Integration times ranged from 400 ms/pixel to 2000 ms/pixel, depending on signal strength and particle size. The entrance slit of the spectrograph was adjusted between 65 μm and 500 μm to balance spectral resolution and signal throughput. A 300 lines/mm ruled grating, blazed at 500 nm and centred at 550 nm, was used, yielding a spectral resolution of 0.96 nm. Each particle was measured over a 3×3 pixel area, with individual pixel dimensions ranging from 0.7 to 1.2 μm, tailored to the particle's size. From each particle the maximum and minimum diameter was measured using the measuring tool in the SEM software. The average diameter of the particle was determined based on this measurement. Background spectra, i.e., without electron beam current, and (if present) cosmic rays were subtracted from the data in the Odemis Software. Measurements for each plastic type were taken on at least two different measurement days to account for any variations due to daily operation of the equipment. A schematic workflow of the SEM-CL measurements is displayed in the SI (Fig. S1).

2.4. Data Analysis

Only measurements with a signal to noise ratio of 10:1 and a minimum intensity of 50 counts (cts.) were included in the analysis. During pre-processing, spectra were smoothed with a Savitzky-Golay filter and intensity was normalised for each spectrum. The data was mean-centred and feature-scaled for principle component analysis (PCA) implementation. Principle component analysis was used to reduce the dimensionality of the data and observe potentially formed clusters. For classification of plastics, two random forest classifiers (RFC) were trained using scikit-learn (Pedregosa et al., 2011). The first was trained on the first 12 principle components (optimized through 5-fold validation to 10 PCs). The second was trained on the entire CL spectrum (512 datapoints for each particle). For both RFCs, the dataset was split into 80 % training and 20 % test data. A stratified approach ensured that both the training and test data contained the same ratio of sub-10 μm and over 100 μm particles as the entire dataset. 400 trees were used in both RFCs.

3. Results

3.1. CL spectra: collection and features

To investigate the potential of SEM-CL for the classification of small microplastics, we collected over 200 CL spectra of particles with a diameter smaller than 10 μm for the five most common plastic types (PE, PP, PA, PS and PET). One difficulty faced by many

Table 1
Overview of the measured microplastic particles with average particle size (Da) and number of measured particles.

Plastic type	Description	Supplier	Average particle size of measured particles (Da in μm)	Number of particles (#)
PE	Milled PE pellet	Nanofract	5.73 ± 1.52	45
PA	Milled PA pellet	TNO	5.30 ± 1.23	45
PET	Milled PET pellet	TNO, Nanofract	7.29 ± 1.05	41
PS	Milled PS pellet	Nanofract	4.66 ± 1.05	50
PP	Milled PP pellet	TNO, Nanofract	6.47 ± 1.78	45
Average			5.84 ± 1.62	

microplastics studies is that test materials are more homogenous in shape and size than those found in the environment (Burns and Boxall, 2018). We investigated particles produced using top-down milling approaches, which result in the generation of irregularly shaped particles that exhibit similar material properties from those found in the environment (Parker et al., 2023; Burns and Boxall, 2018).

In our previous work the studied materials greatly exceeded the size of the interaction volume of the electron beam, allowing us to measure CL spectra with high electron beam voltages (15 kV) and subsequently acquire high CL-intensity signals. In this study, our goal was to measure the spectra of particles smaller than 10 μm in size, which required further optimisation of the analytical depth by tuning CL and SEM parameters prior to spectrum collection. Castaing's formula allows the calculation of the average penetration depth of electrons in homogeneous material (Fedors et al., 1990):

$$z_m = \frac{0.033\left(E_0^{1.7} - E_C^{1.7}\right)A}{\rho Z}$$

Where z_m stands for the analytical depth in μm, E_0 and E_C represent the accelerating voltage and minimum emission voltage in keV, A, the atomic mass, Z, the atomic number and ρ, the density in kg/m^3 respectively.

From the polymers tested, PP has the lowest density with densities ranging from 0.895 to 0.920 g/cm^3(Plastics Europe) Applying

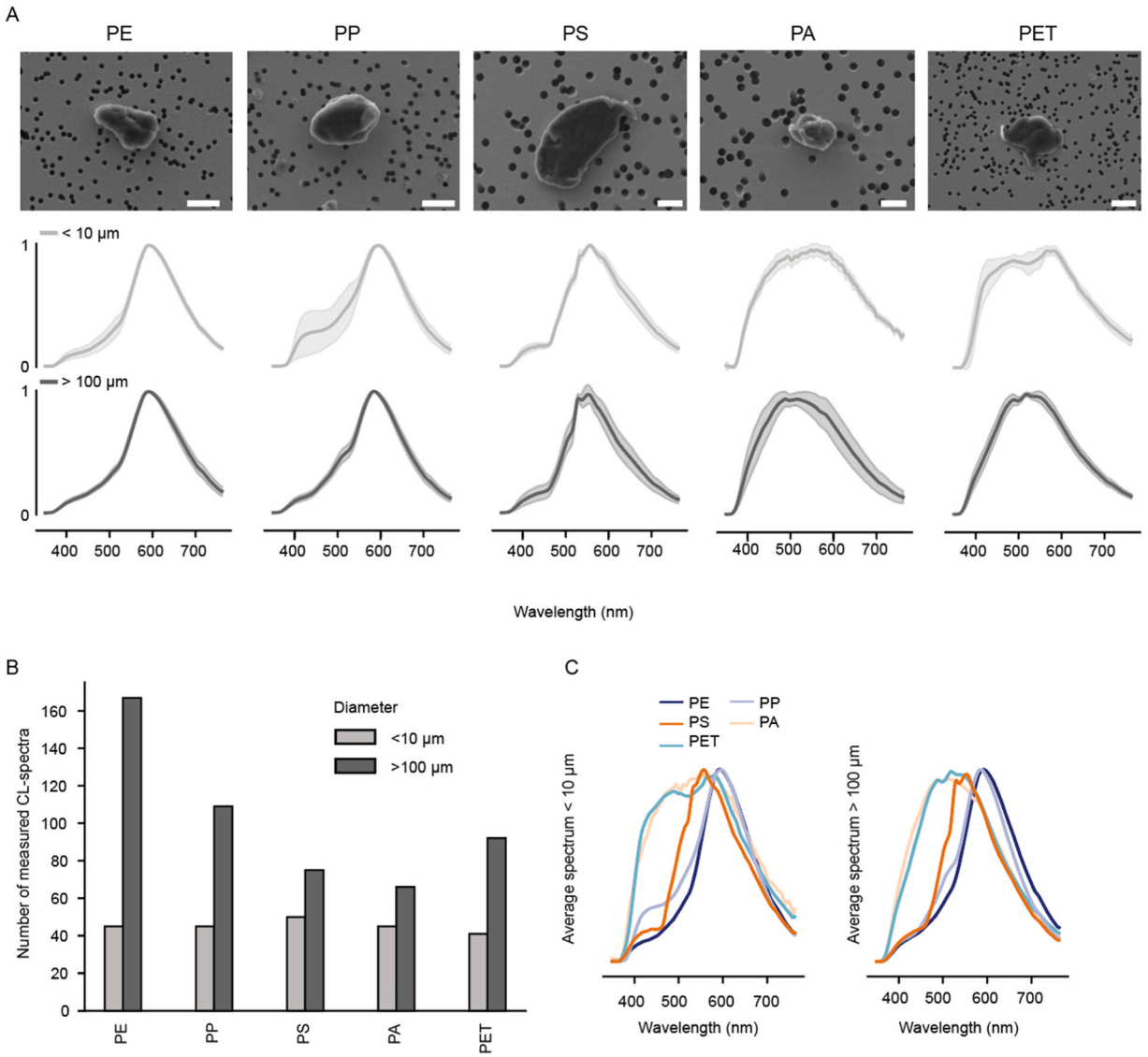

Fig. 1. A: Representative SE images of particles and average CL-spectra (normalised) per plastic type of the microplastics used in the classification model for particles > 100 μm (top, dark-grey line) and < 10 μm (bottom, light-grey line). B: Number of measured CL-spectra per plastic type for particles with equivalent diameter < 10 μm and > 100 μm; C: Average CL-spectra per size range.

Castaing's formula results in a maximum analytical depth of ~7 μm at 15 kV and ~1 μm at 5 kV for PP particles. To prevent signal contamination from substrate, all particles smaller than 10 μm were measured using an acceleration voltage of 5 kV. This lower acceleration voltage resulted in less light being emitted from the materials and thus required further signal optimisation. This was achieved by lengthening exposure times (ranging from 400 ms to 2000 ms), adjusting the input slit to a maximum of 500 μm and

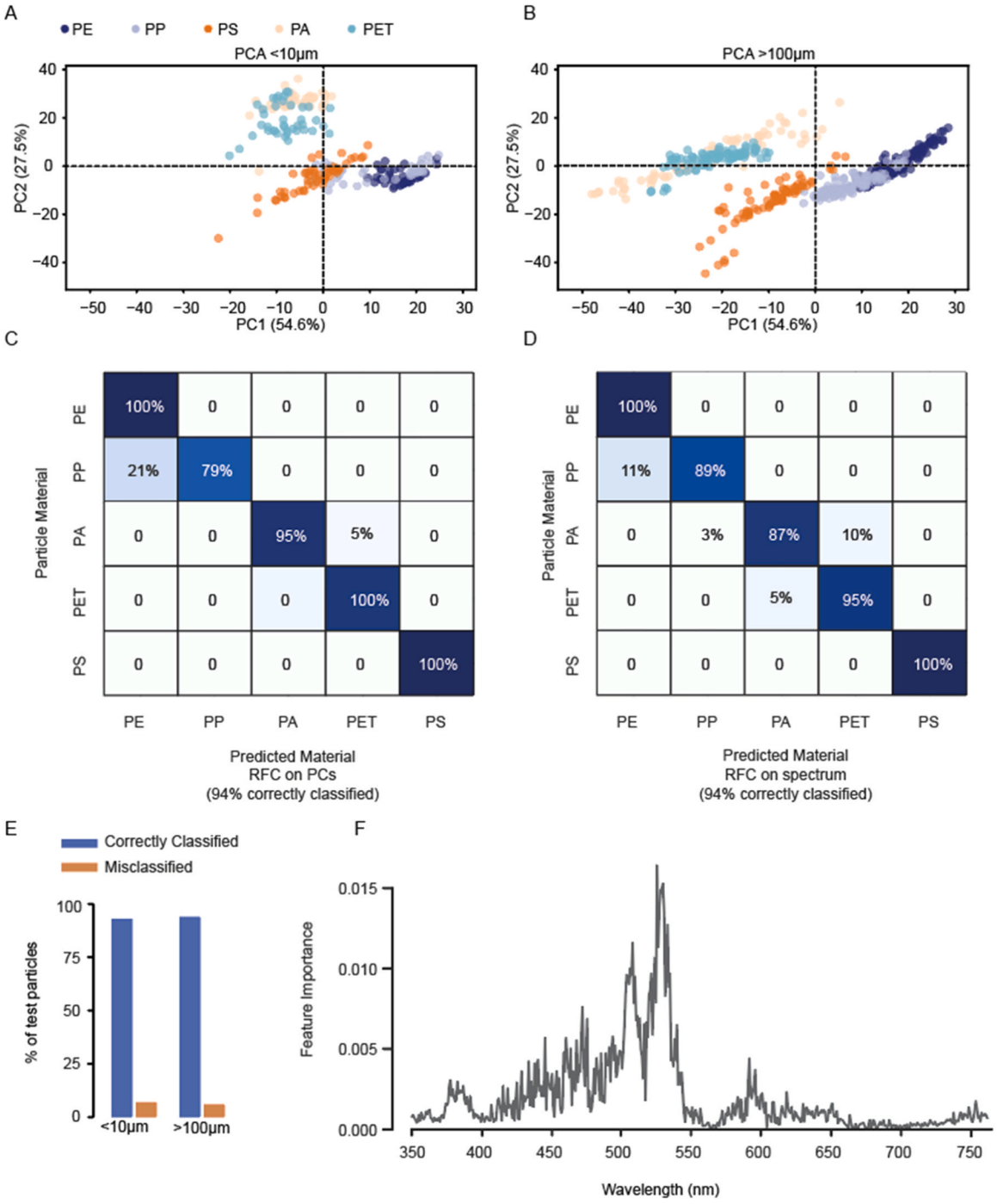

Fig. 2. A: 2D score plot of the first 2 principle components for particles smaller than 10 μm. B: 2D score plots of the first 2 principle components for particles larger than 100 μm. C: Confusion matrix showing the accuracy with which an RFC trained on the first 10 principle components can predict of which polymer a particle consists. D: Confusion matrix showing the accuracy of an RFC if trained on the entire CL spectrum. E: Percentage of < 10 μm and > 100 μm particles correctly classified by the same whole-spectrum RFC. F: Relative feature importance of each wavelength to the whole-spectrum RFC.

decreasing the beam intensity (BI) from 10 to 3. With these adjusted settings, the acquisition times increased from ~8–30 s per particle. Besides preventing substrate contamination, the lower acceleration voltages also induced less damage to particles.

After thorough signal optimisation, CL spectra were collected from < 10 μm particles for the five types of polymers. Representative secondary electron (SE) images and the average normalised CL spectra for each polymer are shown in Fig. 1A for both size fractions, < 10 μm and > 100 μm. A minimum of 40 CL spectra were collected from < 10 μm particles for each polymer type, and compared to the existing measurements of particles > 100 μm (Fig. 1B). Deviation between the individual measurements is displayed as lighter grey fill around the spectra.

The average spectra for both size bins show that spectral features are largely determined by polymer type rather than particle size, suggesting that CL-spectra can be used to distinguish between polymers even for small particles (Fig. 1A, for absolute intensity see S2). However, there are some differences in spectra between < 10 and > 100 μm particles. One is the relative higher intensity values at shorter wavelengths (around 400 nm) in the spectra of PA, PET and PP. This is likely caused by swifter surface oxidation in small particles, for example during the milling process, due to their large exposed surface area relative to particle volume (Linke et al., 2020). Additionally, between 400 and 500 nm, the spectra of < 10 μm PP particles display larger variation. This can be attributed to the presence of the methyl ($-CH_3$) side chain making the particles even more prone to surface oxidation. This likely results in a higher presence of carbonyl (CO) groups for small PP particles, contributing to CL intensity around 415 nm due to the relaxation of excited carbonyl radicals (CO*). PA and PET already contain CO as a functional group in the polymer backbone, perhaps explaining why there is less deviation observed for these polymers compared to the CL spectra of the bulk measurements (particles >100 μm). For PET, it appears that the main peak is shifted more towards 600 nm. One possible explanation is that with smaller particle sizes new energy levels are introduced by material defects, affecting the CL emission of PET. Average CL spectra before normalisation, displaying the mean measured intensities, are shown in the Supplementary Information (see Fig. S2). For most polymers, the average peak intensity was similar for both particle size groups, though higher for PE and PP than for PA and PET. Only the < 10 μm PS particles produced far lower intensity spectra than their > 100 μm counterparts.

Despite these size-dependent differences, overlaying the average normalised spectra for each polymer type shows that even for these small particles, different polymers produce distinct CL spectra with specific spectral shapes and (maximum) peak positions (Fig. 1C), in line with our previous findings and those of Pakzad et al.(2014).

3.2. PCA results

To verify whether the CL spectra of small particles are indeed unique enough to differentiate between plastic types, principal component analysis (PCA) was performed on the dataset (Fig. 2A and B). 2D score plots show that the first two principle components (PCs) allow the creation of three groups; PE with PP, PET with PA, and PS. The overlap of PE and PP is in accordance with previous work by Qiao et al., where CL spectra of PP and PE were found to be organized along the same elementary components although with different relative contributions of the individual peaks (Qiao et al., 2016). Compared to PE, the individual PP points are more scattered in the plot, corresponding to the higher variation found in the PP dataset. PC2 allows the separation of the scores of the second cluster, PET with PA, from the others. These results suggest that classification based on PCs could lead to successful differentiation between polymer types, but that a non-linear approach would be required, with the most challenging distinction lying in differentiating between PP and PE or PA and PET.

3.3. Model development & results

To develop a classification model, a method was used which incorporates supervised learning and the ability to form non-linear boundaries. In our previous work, we used an artificial neural network (ANN) to classify the polymer types based on their CL spectra. ANNs do constitute a powerful approach, however, given the large amounts of data that are required for reliable ANNs and the labour-intensive process of obtaining CL spectra from small particles, as well as the relatively high computational expense of ANNs and the lack of insight they can provide into the process used for the classification, we proceeded to use a random forest classifier (RFC). The first RFC was trained on the first 10 PCs. This number was arrived at through 5-fold cross-validation of how many PCs continued to increase accuracy. The cumulative variance explained per PC (see SI Fig. S3), shows that with the first four PCs an explained variance of 93.5 % is obtained and that with 10 PCs, more than 95 % of the input data can be explained. The classifier performed well, as an average of 96 % of particles were classified as the correct polymer over 10 runs (each with different test-training data split) (Fig. S5). As can be seen in the confusion matrix (Fig. 2D), misclassifications most often occurred for PP.

For a classification method to be of practical use, particularly across different users, required pre-processing should be minimised. In order to use the RFC based on principle component analysis, new data would need to be transformed in accordance with the PCs of the initial dataset. To promote ease of use in different scenarios, a second RFC was therefore trained on the full normalised CL spectrum of the particles (Fig. 2D), increasing the number of datapoints per particle from 12 to 512. This RFC also performed well, with an average accuracy of 94 % over 10 runs, and requires no data-specific pre-processing other than smoothing and normalisation of the input data. These classifiers confirm that the spectra of the < 10 μm and > 100 μm particles for each polymer are similar enough for accurate classification, as an RFC can accurately classify both < 10 μm and > 100 μm particles using the same rules (Fig. 2E).

The use of the RFC classifier over the entire spectrum allows access to the relative contribution of each wavelength of the spectrum to the classification outcome (Fig. 2F). Peaks are visible around 505 and 530 nm, corresponding to the regions of the spectra that show the biggest differences between the three groups (PP & PE, PET & PA, PS) as visible in the PCA.

In real-world applications, a classifier can be expected to face CL spectra of contaminating particles upon which it has not been

trained. To deal with this case, a 'certainty threshold' was applied. Upon classification of a particle, the RFC produces a probability of this particle belonging to each polymer included in the model. Particles that did not cross this certainty threshold were labelled 'unclassified' and considered possible contaminants. To test appropriate values for the certainty threshold, the CL spectra of three common contaminant particles were measured: kaolin (clay mineral), talc (naturally occurring mineral) and titanium dioxide (TiO_2, filler material for plastics) (Fig. 3A). These spectra were fed into the existing whole spectrum RFC and subsequently classified. As expected, contaminants were assigned lower probabilities of belonging to any polymer class, as were plastic particles that were incorrectly classified (Fig. 3B). Fig. 3C compares the true positive rate (the frequency with which a plastic particle was labelled correctly) and the false positive rate (the frequency with which either a true contaminant was classified as a plastic, or a plastic particle was classified incorrectly) depending on the value set for the certainty threshold. A certainty threshold of 0.75 allows separation of contaminants and plastics in this model.

In conclusion, a random forest classifier is a computationally light way to automatically classify the material of particles down to

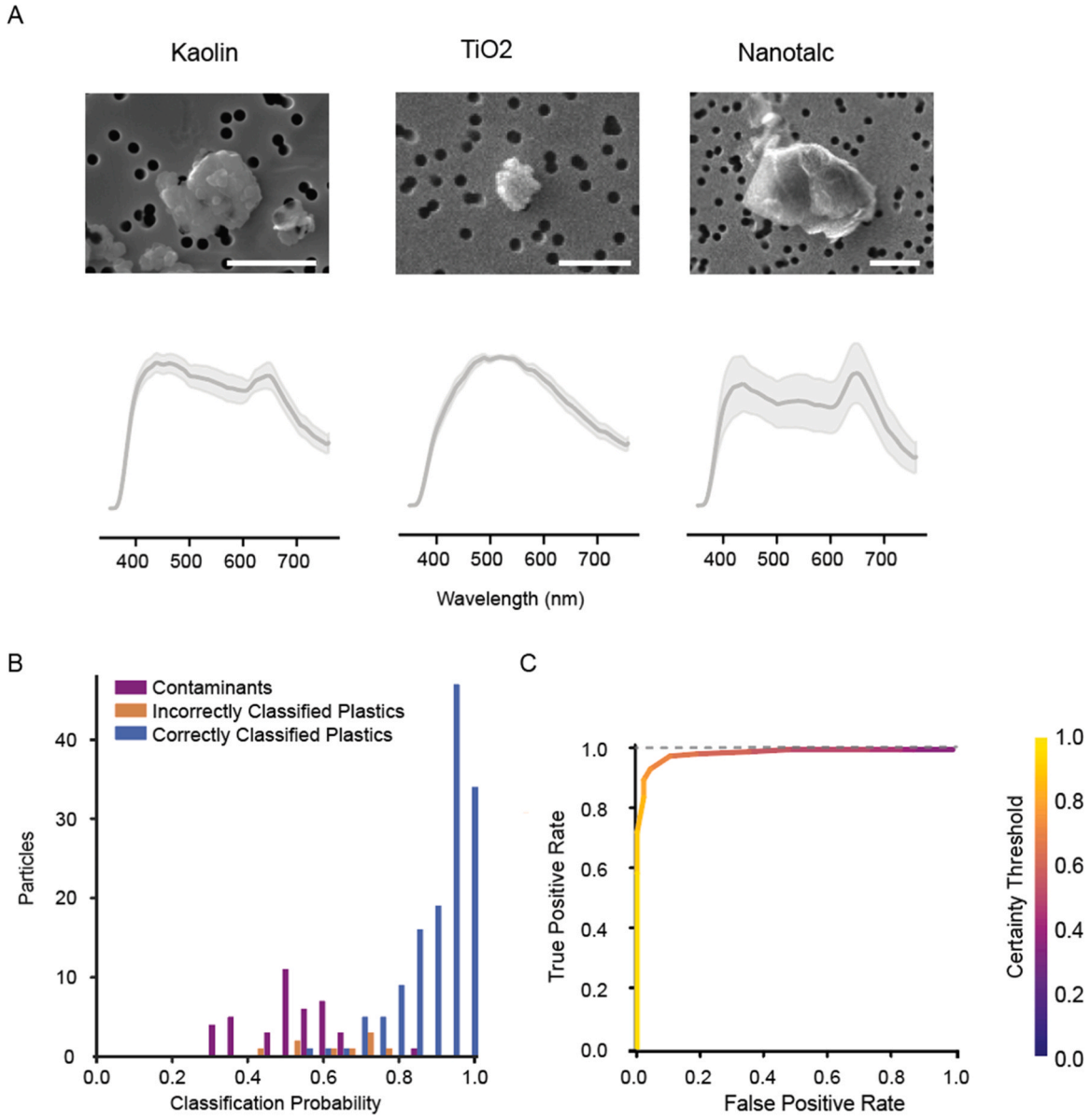

Fig. 3. A: Average CL spectra for < 10 μm particles of three common contaminants: kaolin, TiO_2 and talc. B: The RFC assigns each particle to a polymer with a certain probability. This probability is lower for contaminants (purple) and incorrectly classified plastics (orange) than for correctly classified plastics (blue). C: ROC curve displaying how the true positive rate (frequency with which a plastic is labelled as the correct polymer) varies with the false positive rate (frequency with which an incorrectly labelled plastic or contaminant is labelled a polymer) depending on the certainty threshold applied.

sub-micron size region and can be used on minimally processed spectra. Including a certainty threshold allows the experimenter to determine which true/false positive rate is appropriate depending on the sample and application.

4. Conclusions & outlook

This study explores the potential of scanning electron microscopy coupled with cathodoluminescence (SEM-CL) for the classification of small microplastics based on polymer. CL spectra were successfully collected for particles smaller than 10 μm across five common plastic types (PE, PP, PA, PS, and PET). To ensure that test materials closely resembled environmental microplastics, particles were used that were created using top-down milling approaches. Signal optimisation of measurement parameters was crucial to successfully obtaining CL spectra of particles smaller than 10 μm, where lower acceleration voltages (5 kV) minimized beam-induced damage and required longer exposure times. Principal component analysis (PCA) revealed three distinct clusters where PE grouped with PP, PET with PA, and PS grouped alone. The overlap observed between PE and PP aligns with previous findings, indicating similar elementary components but varying peak contributions. The second principal component (PC2) effectively separates PET and PA from other polymers. These results show that principle components can differentiate between some spectral characteristics of polymer types. A random forest classifier could be trained successfully classify spectra into plastic type based on both principle components and the minimally processed CL spectrum itself. Testing the full spectrum classifier on common contaminants demonstrated its ability to use a certainty threshold to distinguish between target microplastics and contaminant particles which it had not previously encountered.

Several steps were taken to maximise the relevance of this classifier for environmental samples of microplastics; the five selected plastics constitute an estimated 63 % of plastic production, the top-down milling produces irregularly shaped particles, and the uncertainty threshold allows the experimenter to determine which sensitivity is appropriate for the sample. To further scale this classifier from proof of principle to a robust tool would first require extending the database upon which the classifier is trained. For instance, additional polymers could be added, and robustness would be greatly improved by including CL spectra from different SEMs in different labs. Including even smaller particles, down to the nanoplastics range, would allow even broader use, however, producing environmentally relevant nanoplastic test materials is highly challenging and commonly used methods like mechanical fragmentation, photodegradation, sonication, laser ablation, and thermal degradation often yield particles with a wide range of sizes and shapes, making it difficult to separate solely the nanoplastic fraction for use as test material. Nevertheless, the theoretical use of SEM-CL for nanoplastics is one advantage of this method. Finally, CL spectra of a set of contaminants could be added to the training set to allow the classifier to not only register that a contaminant has been measured, but to identify it. These measures would allow the classifier to respond with higher accuracy to different complex scenarios.

In a typical environmental study, analysing thousands of particle spectra manually for plastic identification and counting is extremely labour-intensive and prone to human bias. High throughput (plastic) particle analysis requires techniques to automatically identify plastic types based on spectral features as is already seen in, for example, spectral matching algorithms for automated chemical identification based on FTIR or Raman spectroscopy. For this SEM-CL technique to be applicable for environmental studies on the presence of nanoplastics, it is crucial to test the potential for automation. Since the acquisition times are relatively short with average acquisition times of 30 s per particle, SEM-CL has a high potential for automation. Furthermore, automation in collaboration with a variety of functional attachments often equipped in SEM systems (e.g. EDX, BSE, EBSD) allows for a comprehensive analysis tool of multiple characteristics within the same microregion of a sample, including different surface morphologies, elemental compositions, crystallographic features and the potential for single particle identification of nanoplastics.

CRediT authorship contribution statement

Höppener Elena: Writing – original draft, Visualization, Methodology, Investigation, Data curation. **Yoe Laurine:** Writing – review & editing, Methodology, Investigation. **Leighton Alexandra:** Writing – original draft, Visualization, Software, Methodology, Investigation, Data curation, Conceptualization. **Sieger Henke:** Writing – review & editing, Supervision, Project administration, Funding acquisition. **van Amelrooij Edward:** Writing – review & editing, Methodology. **Parker Luke:** Writing – review & editing, Supervision, Methodology, Conceptualization.

Declaration of Competing Interest

The authors declare the following financial interests/personal relationships which may be considered as potential competing interests: Elena Hoppener reports equipment, drugs, or supplies was provided by Plastics Europe. If there are other authors, they declare that they have no known competing financial interests or personal relationships that could have appeared to influence the work reported in this paper.

Acknowledgements

Some of the particles used in this work were produced as part of the BRIGID, MOMENTUM and MOMENTUM2.0 projects. The MOMENTUM project was made possible by ZonMw Programme Microplastics and Health, and Health-Holland, Top Sector Life Sciences & Health (project number 458001101). The MOMENTUM2.0 is funded by ZonMw Programme Microplastics and Health (project number 4580012310002). The BRIGID project (Grant Number 001) is funded by Plastics Europe. The funding organisations had no

influence on the work presented in the manuscript.

During the preparation of this work the authors used Co-Pilot in order to improve language and readability. After using this tool/service, the authors reviewed and edited the content as needed and take full responsibility for the content of the publication.

Appendix A. Supporting information

Supplementary data associated with this article can be found in the online version at doi:10.1016/j.eti.2025.104583.

Data availability

Data will be made available on request.

References

Burns, E.E., Boxall, A.B.A., 2018. Microplastics in the aquatic environment: evidence for or against adverse impacts and major knowledge gaps (Nov.). Environ. Toxicol. Chem. 37 (11), 2776–2796. https://doi.org/10.1002/ETC.4268.

Campen, M., et al., 2024. Bioaccumulation of microplastics in decedent human brains assessed by pyrolysis gas chromatography-mass spectrometry. Res. Sq. https://doi.org/10.21203/rs.3.rs-4345687/v1.

European Commission, "Pathway to a healthy planet for all. EU action plan: 'Towards zero pollution for air, water and soil,'" *COM(2021) 400 Final*, p. 22, 2021, [Online]. Available: ⟨https://eur-lex.europa.eu/resource.html?uri=cellar:a1c34a56-b314-11eb-8aca-01aa75ed71a1.0001.02/DOC_1&format=PDF⟩.

Fedors, R.F., et al., 1990. Energy table for EDS analysis. J. Polym. Sci. Part A Polym. Chem. 38 (6), 147–154.

Gasperi, J., et al., 2018. Microplastics in air: are we breathing it in? Curr. Opin. Environ. Sci. Heal 1, 1–5. https://doi.org/10.1016/j.coesh.2017.10.002.

Geyer, R., Jambeck, J.R., Law, K.L., 2017. Production, use, and fate of all plastics ever made (Jul.). Sci. Adv. 3 (7), e1700782. https://doi.org/10.1126/sciadv.1700782.

Höppener, E.M., (Sadegh) Shahmohammadi, M., Parker, L.A., Henke, S., Urbanus, J.H., 2023. Classification of (micro)plastics using cathodoluminescence and machine learning (Feb.). Talanta 253, 123985. https://doi.org/10.1016/J.TALANTA.2022.123985.

ISO/TR 21960:2020(en), Plastics — Environmental aspects — State of knowledge and methodologies." https://www.iso.org/obp/ui/#iso:std:iso:tr:21960:ed-1:v1:en (accessed Dec. 21, 2022).

Jiang, R., Yao, Y., Guan, J., Shen, J., Lu, H., Li, M., 2024. Application of SEM-CL system in the characterization of material microstructures. Front. Mater. Sci. 18 (4), 1–19. https://doi.org/10.1007/s11706-024-0709-5.

Koelmans, A.A., Mohamed Nor, N.H., Hermsen, E., Kooi, M., Mintenig, S.M., De France, J., 2019. Microplastics in freshwaters and drinking water: critical review and assessment of data quality (May). Water Res 155, 410–422. https://doi.org/10.1016/J.WATRES.2019.02.054.

Leslie, H.A., Depledge, M.H., 2020. Where is the evidence that human exposure to microplastics is safe? (Sep.). Environ. Int. 142, 105807. https://doi.org/10.1016/J.ENVINT.2020.105807.

Leslie, H.A., van Velzen, M.J.M., Brandsma, S.H., Vethaak, A.D., Garcia-Vallejo, J.J., Lamoree, M.H., 2022. Discovery and quantification of plastic particle pollution in human blood (May). Environ. Int. 163, 107199. https://doi.org/10.1016/j.envint.2022.107199.

Li, M., et al., 2025. Unraveling post-growth mechanisms of monolayer CsPbBr3 nanocubes: laser-enhanced transformations and cathodoluminescence-electron microscopy correlations. J. Energy Chem. 100, 146–156. https://doi.org/10.1016/j.jechem.2024.08.021.

Linke, A., Hinrichs, J., Kohlus, R., 2020. Impact of the powder particle size on the oxidative stability of microencapsulated oil. Powder Technol. 364, 115–122. https://doi.org/10.1016/j.powtec.2020.01.077.

Mandemaker, L.D.B., Meirer, F., 2023. Spectro-microscopic techniques for studying nanoplastics in the environment and in organisms. Angew. Chem. Int. Ed. 62 (2). https://doi.org/10.1002/anie.202210494.

Nair, H.T., Perumal, S., 2022. Trophic transfer and accumulation of microplastics in freshwater ecosystem: risk to food security and human health. Int. J. Ecol. 2022 (Table 1). https://doi.org/10.1155/2022/1234078.

Nikon, "The Diffraction Barrier in Optical Microscopy." ⟨https://www.microscopyu.com/techniques/super-resolution/the-diffraction-barrier-in-optical-microscopy⟩ (accessed Mar. 28, 2025).

OECD, "Plastic pollution is growing relentlessly as waste management and recycling fall short, says OECD," 2022. ⟨https://www.oecd.org/en/about/news/press-releases/2022/02/plastic-pollution-is-growing-relentlessly-as-waste-management-and-recycling-fall-short.html⟩ (accessed Jan. 24, 2025).

Pakzad, A., Stowe, D.J., Nagy, S., Mantei, J.R., Green, J.-B., 2014. Cathodoluminescence of polymeric materials (Aug.). Microsc. Micro 20 (S3), 1996–1997. https://doi.org/10.1017/S1431927614011714.

Palamara, E., et al., 2020. Applying SEM-Cathodoluminescence imaging and spectroscopy as an advanced research tool for the characterization of archaeological material. Microchem. J. 158 (September 2019), 105230. https://doi.org/10.1016/j.microc.2020.105230.

L. Parker, E.M. Höppener, S. Henke, A. Boersma, and A.M. Brunner, "Zenodo Sample Passports MOMENTUM Test Materials," 2024. [Online]. Available: ⟨https://doi.org/10.5281/zenodo.13683074⟩.

Parker, L.A., et al., 2023. Protocol for the production of micro- and nanoplastic test materials. Micro Nanoplastics 3 (1). https://doi.org/10.1186/s43591-023-00058-2.

Pedregosa, F., et al., 2011. Scikit-learn: machine learning in Python. J. Mach. Learn. Res. 12, 2825–2830.

Pei, W., Hu, R., Liu, H., Wang, L., Lai, Y., Sep. 2023. Advanced Raman spectroscopy for nanoplastics analysis: progress and perspective. TrAC Trends Anal. Chem. 166, 117188. https://doi.org/10.1016/j.trac.2023.117188.

Phuong, N.N., et al., 2021. Highlights from a review of microplastics in marine sediments. Sci. Total Environ. 777. https://doi.org/10.1016/j.scitotenv.2021.146225.

Plastic Europe, "Plastics – the fast Facts 2024," 2024.

Plastics Europe, Polyolefins, *Properties of polyolefins*. https://plasticseurope.org/plastics-explained/a-large-family/polyolefins/#:~:text=PP(polypropylene)%3A The density,0.895 and 0.92g%2Fcm3.

Qian, B.Y. Naixin, Gao, Xin, Lang, Xiaoqi, Deng, Huiping, Teodora Maria Bratu, Chen, Qixuan, Phoebe Stapleton, Min, W., 2023. Rapid single- particle chemical imaging of nanoplastics by SRS microscopy. Proc. Natl. Acad. Sci. 121. https://doi.org/10.1073/pnas.

Qiao, B., Teyssedre, G., Laurent, C., 2016. Electroluminescence and cathodoluminescence from polyethylene and polypropylene films: spectra reconstruction from elementary components and underlying mechanisms (Jan.). J. Appl. Phys. 119 (2), 024103. https://doi.org/10.1063/1.4939824.

K. Rasmussen *et al.*, *Titanium Dioxide, NM-100, NM-101, NM-102, NM-103, NM-104, NM-105: Characterisation and Physico- Chemical Properties.* 2014.

Rathenau, "Belanghebbenden bij het voorzorgsprincipe," 2020. ⟨https://www.rathenau.nl/nl/kennis-voor-transities/belanghebbenden-bij-het-voorzorgsprincipe⟩ (accessed Jan. 24, 2025).

Schymanski, D., et al., 2021. Analysis of microplastics in drinking water and other clean water samples with micro-Raman and micro-infrared spectroscopy: minimum requirements and best practice guidelines. Anal. Bioanal. Chem. 413 (24), 5969–5994. https://doi.org/10.1007/s00216-021-03498-y.

Sunny, A.R., et al., 2025. Microplastics in aquatic ecosystems: a global review of distribution, ecotoxicological impacts, and human health risks. Water (Switz.) 17 (12), 1–21. https://doi.org/10.3390/w17121741.

Thornton Hampton, L.M., et al., 2022. Characterizing microplastic hazards: which concentration metrics and particle characteristics are most informative for understanding toxicity in aquatic organisms? Micro Nanoplastics 2 (1). https://doi.org/10.1186/s43591-022-00040-4.

Uddin, S., Fowler, S.W., Uddin, M.F., Behbehani, M., Naji, A., 2021. A review of microplastic distribution in sediment profiles. Mar. Pollut. Bull. 163 (ember 2020), 111973. https://doi.org/10.1016/j.marpolbul.2021.111973.

Vethaak, A.D., Legler, J., 2021. Microplastics and human health (Feb.). Science (80.) 371 (6530), 672–674. https://doi.org/10.1126/science.abe5041.

Wei, Z., Wang, Y., Wang, S., Xie, J., Han, Q., Chen, M., 2022. Comparing the effects of polystyrene microplastics exposure on reproduction and fertility in male and female mice. Toxicology 465 (December 2021), 153059. https://doi.org/10.1016/j.tox.2021.153059.

Wright, S.L., Gouin, T., Koelmans, A.A., Scheuermann, L., 2021. Development of screening criteria for microplastic particles in air and atmospheric deposition: critical review and applicability towards assessing human exposure. Micro Nanoplastics 1 (1), 1–18. https://doi.org/10.1186/s43591-021-00006-y.

Zhou, Q., Li, D., Wang, T., Hu, X., 2025. Quantification of micro- and nano-plastics in atmospheric fine particles by pyrolysis-gas chromatography-mass spectrometry with chromatographic peak reconstruction. J. Hazard. Mater., 124046 https://doi.org/10.1016/j.jhazmat.2025.137292.

Zimmermann, L., Göttlich, S., Oehlmann, J., Wagner, M., Völker, C., 2020. What are the drivers of microplastic toxicity? Comparing the toxicity of plastic chemicals and particles to Daphnia magna. Environ. Pollut. 267. https://doi.org/10.1016/j.envpol.2020.115392.